IEEE Access
Multidisciplinary | Rapid Review | Open Access Journal

Received 24 September 2023, accepted 3 October 2023, date of publication 13 October 2023, date of current version 19 October 2023.

Digital Object Identifier 10.1109/ACCESS.2023.3323595

RESEARCH ARTICLE

Gabor Filter-Based Multi-Scale Dense Network Hyperspectral Remote Sensing Image Classification Technique

CHAOZHU ZHANG, SHENGRONG ZHU, DAN XUE, AND SONG SUN
Department of Electronics Electricity and Control, Qilu University of Technology, Jinan 250000, China
Corresponding author: Dan Xue (10431210553@stu.qli.edu.cn)

ABSTRACT Since hyperspectral remote sensing images are three-dimensional data cubes with spatial and spectral information, with many wavebands and high inter-band correlation, the number of training samples required for classification is greatly increased. In order to achieve better classification of hyperspectral remote sensing images with small samples, this paper proposes a hyperspectral remote sensing image classification method based on Multi-Scale Dense Network (MSDN) with 3D Gabor filter. The method extracts the texture features of hyperspectral remote sensing images by using 3D Gabor filter; then extracts the spatial spectral features of hyperspectral remote sensing images at different scales in both horizontal and vertical directions by using Multiscale Dense Network; and finally achieves the classification of hyperspectral remote sensing images by using Softmax classifier. The introduction of 3D Gabor filter in this method can improve the extraction effect of the features of hyperspectral remote sensing images, and at the same time reduce the dependence of the multiscale dense network on the labeled samples in the classification of hyperspectral remote sensing images. Experiments are conducted on three publicly available hyperspectral remote sensing datasets, and the experimental results are compared with other classification methods to prove that the method has better classification performance.

INDEX TERMS Hyperspectral remote sensing image classification, multiscale dense network, small sample, three-dimensional.

I. INTRODUCTION

Each pixel in hyperspectral remote sensing image data has hundreds of bands, and it contains spatial and spectral information of the features, thus forming a high-dimensional data structure. Compared with ordinary RGB images, hyperspectral remote sensing images can identify the information of land features more finely and accurately.

Early hyperspectral remote sensing image classification methods used feature extraction combined with classifiers for classification. Among them, Xie et al. [1] proposed the use of orthogonal subspace projection, which projects a certain vector of pixels onto a sub-space of signals that are orthogonal to the undesired presence and projects the reserved signal onto the signal of interest, resulting in a single-component image. This method excludes undesired or interfering spectral signals while reducing the dimensionality of the data. Support vector machines are based on statistical learning theory and are better able to solve practical problems such as small samples, high dimensionality, nonlinearity and local minima. Melgani used support vector machine (SVM) to classify hyperspectral remote sensing images, and the experimental results showed that the algorithm showed good performance with very limited training samples [2]. Chen et al. [3] proposed a method for classification using spatially dominant features. This is because it is considered that large neighborhood regions can cause the classifier to be considered as having too large an input dimension and contain too much redundancy. Therefore, in the first layer, Principal Component Analysis (PCA) is introduced to compress the whole image to reduce the data dimensionality to an acceptable scale while preserving the spatial information, and then the

The associate editor coordinating the review of this manuscript and approving it for publication was Donato Impedovo.

compressed hyperspectral data are used for spatial feature extraction with SAEs of different scales.

In recent years, with the development of computer technology, people have made great breakthroughs in the research of deep learning, which has extremely wide applications in images and text. Deep learning networks are generally multilayer, and feature extraction using multilayer networks can obtain more abstract information. Yue et al. [4] introduced a deep CNN model to extract spatial features with the help of principal component analysis (PCA) and logistic regression. Xu et al. [5] integrated HSI data and multisensor data to improve the classification performance, where the spectral and spatial features of HSI data were extracted by 1D CNN and 2D CNN, respectively. In addition [6], several literatures use off-the-shelf CNN models, including AlexNet [7], VGGNet [8], GoogleNet [9] and ResNet [10] for deep spatial feature extraction on hyperspectral image datasets and achieve high classification accuracy. Shen et al. [11] proposed an end-to-end hybrid convolutional neural network for hyperspectral image classification. Firstly, the 3D, 2D and 1D convolutional modules are applied for joint feature extraction of spatial and spectral information, respectively. Secondly, a new 3D multi-scale feature fusion strategy is proposed to fuse the high-level and low-level features in order to ensure the adequacy of the features.

Although deep learning networks have gained significant advantages in the field of hyperspectral remote sensing image classification, however, they still suffer from the problem that fine features are often lost or even disappeared in large quantities during the depth transfer process. In order to improve deep learning networks and enhance their classification capabilities, the concept of multiscale began to emerge. Zhaokui Li et al. [12] proposed a new deep multilayer fusion dense network (MFDN) to improve the performance of HSI classification. The proposed MFDN extracts both spatial and spectral features based on different sample input sizes, which can extract rich spectral and spatially relevant information. Spatial features are extracted from low-dimensional 3-D HSI data by 2-D convolution, 2-D dense block and mean. Second, excellent hyperspectral classification performance is achieved by directly extracting spectral features from the raw 3-D HSI data through 3-D convolution, 3-D dense blocks, and averaging pooling layers. Zhang et al. [13] applied multiscale dense networks to hyperspectral remote sensing image classification, making full use of the information of different scales in the network structure and combining the scale information of the whole network to achieve feature extraction in two dimensions and generate feature maps of low, medium and high levels based on the first layer of the network. Multiscale dense networks have been widely used in the field of hyperspectral remote sensing image classification because they are well suited for hyperspectral remote sensing image characteristics. Xu et al. [14] designed a HSI multiscale spectral spatial CNN based on a novel image classification framework. The network is able to integrate multiple receptive field fusion features with different levels of multi-scale spatial features to improve the classification ability. Fırat et al. [15] proposed a method in which the Hybrid 3D/2D Complete Inception module and the Hybrid 3D/2D CNN method are used together has been proposed to solve the HRSIs classification problem. In the proposed method, multi-level feature extraction is performed by using multiple convolution layers with the Inception module. This improves the performance of the network. Ari et al. [16] proposed a method consisting of a combination of multipath Hybrid CNN and a Squeeze and Excitation (SE) network for HSIC. Features extracted with different kernel sizes in the multipath method are used together to extract richer feature information from HSI in this proposed method (PM).

Although the multiscale dense network has shown excellent results in the field of hyperspectral remote sensing image classification, it also has disadvantages, such as strong dependence on labeled samples and slow running speed because the network structure is too complicated. And the 3D Gabor filter can extract some internal information such as the edges of the image, the direction and size of the image texture, etc. Applying the Gabor filter to hyperspectral remote sensing image classification can further extract the spatial features of the image and reduce the dependence of the network model on the samples [17].

Therefore, this paper proposes a multiscale dense network based on 3D Gabor filter for hyperspectral remote sensing image classification. The combination of the two can extract more accurate features of hyperspectral remote sensing images: the 3D Gabor filter can extract the spatial features of hyperspectral remote sensing images, while the multi-scale dense network can extract the frequency features of hyperspectral remote sensing images. The combination of the two can obtain more comprehensive and accurate hyperspectral remote sensing image features, which makes the recognition and classification tasks more excellent. Secondly, it can improve the noise resistance: the three-dimensional Gabor filter has strong noise resistance, which can reduce the noise interference in the hyperspectral remote sensing images and improve the accuracy of recognition and classification. And the multi-scale dense network can improve its robustness and stability against interference by suppressing noise. Further it can reduce the feature dimensionality: as the number of hyperspectral remote sensing image bands increases, the feature dimensionality also increases, which puts more pressure on the computation and storage. Multi-scale dense networks combined with 3D Gabor filters can extract more accurate features and help optimize features, thus reducing feature dimensionality, improving computational efficiency and accuracy, and also increasing image processing speed. Traditional hyperspectral remote sensing image processing methods consume a lot of time and resources, while multi-scale dense networks combined with 3D Gabor filters can reduce redundant calculations and improve processing speed and efficiency.

The rest of the paper is organized as follows. In Section II, the structure of the multiscale dense network mentioned in

the article, the basic principles of the 3D Gabor filter, the 3D Gabor filter bank designed in the article and the experimental evaluation metrics are described. In Section III, experiments on three publicly available hyperspectral remote sensing image datasets are described and compared with other methods to verify the effectiveness of the method proposed in the article. Section IV gives the conclusion of the paper.

II. MATERIALS AND METHODS

A. STRUCTURE OF MULTI-SCALE DENSE NETWORKS

Multiscale dense networks (MSDN) are improved deep learning networks that can extract features at different scales. Features in hyperspectral remote sensing images have different scales of spatial location relationships, and the use of multi-scale dense networks helps to extract the location information of these features. Also the multi-scale dense network uses Dense Block to enhance the connectivity between layers and can use Multi-Scale Dense Connection matrix for multi-layer feature fusion. This helps to improve the expressiveness and robustness of the features and can eliminate the gradient disappearance and gradient explosion problems. In addition to this multi-scale dense network also supports the addition of new dense blocks to the network structure in order to achieve deeper or wider networks, which helps to extend the structure of the network and thus apply to more complex hyperspectral image classification problems. The specific structure of the MSDN network is shown in Table 1, and the spectral dimension of the hyperspectral remote sensing image is downscaled using principal component analysis before inputting into the network, and the first 30 principal components are retained to reduce data redundancy.

TABLE 1. Sample size of Indian Pines dataset.

Layers	Output Size	SMSDN（S=3，K=32）
3D Convolution	25*25*30	3*3*3 conv with stride 1
3D MaxPooling	12*12*15	3*3*3 max pool with stride 2
Dense block 1	12*12*15	$\begin{bmatrix} 1*1*1 \\ 3*3*3 \end{bmatrix} *3$
Transition layer 1	12*12*15 6*6*7	1*1*1 conv 1*1*1 average pool with stride 2
Dense block 2	6*6*7	$\begin{bmatrix} 1*1*1 \\ 3*3*3 \end{bmatrix} *4$
Transition layer 2	6*6*7 3*3*3	1*1*1 conv 1*1*1 average pool with stride 2
Dense block 3	3*3*3	$\begin{bmatrix} 1*1*1 \\ 3*3*3 \end{bmatrix} *3$
Classification layer	1*1*1	Global average pool softmax

B. THREE-DIMENSIONAL GABOR FILTER SET

Gabor filter is a filtering method widely used in image processing and analysis. Its basic principle is to construct a complex filter using sine and cosine functions, which can be used to extract image texture information in different directions and on different scales, respectively. In hyperspectral remote sensing image classification, Gabor filter is also widely used as a preprocessing tool for feature extraction of hyperspectral images. The Gabor filter can perform feature extraction in both direction and scale. One-dimensional Gabor filters are mainly used to process one-dimensional data, such as sound. Two-dimensional Gabor filters make the most widely used filters and can be extended to meet specific needs. In hyperspectral remote sensing image classification, Gabor filters are usually used to extract texture information from images by selecting different filter parameters to suit different image features. Commonly used parameters include the center frequency, bandwidth, orientation and phase of the filter. Since the hyperspectral image is a three-dimensional cubic data structure, the two-dimensional Gabor filter cannot extract its texture feature information and spectral information at the same time. In order to be able to extract the texture information of the hyperspectral image while preserving its spectral features, it is necessary to upgrade the two-dimensional Gabor filter to a three-dimensional Gabor filter.

The 3D Gabor filter is a complex filter constructed using sine and cosine functions, which can be used to extract image texture information in different directions and on different scales, respectively. Specifically, the 3D Gabor filter can be adapted to different image textures and features by adjusting its parameters such as spatial frequency, orientation, and bandwidth. In hyperspectral image classification, the 3D Gabor filter can extract texture features of hyperspectral images in different directions and scales.

The three-dimensional Gabor filter is calculated as

$$G(x,y,z) = \frac{1}{(2\pi)^{3/2}\sigma_x\sigma_y\sigma_z} \times \exp\left(-\frac{1}{2}\left(\left(\frac{x'}{\sigma_x}\right)^2 + \left(\frac{y'}{\sigma_y}\right)^2 + \left(\frac{z'}{\sigma_z}\right)^2\right)\right) \times \exp\left(2i\pi\left(xf_x + yf_y + zf_z\right) + \varphi\right) \quad (1)$$

where $x' = x\cos\theta + y\sin\theta, y' = -x\cos\theta + y\sin\theta, z' = z$ denote the three-dimensional Gabor filters and $G(x,y,z)$ denotes the width of the spatial spectrum. The directions of the filters are indicated by θ and φ. $[x,y,z]$ denotes the coordinates of a point of the original image data, after rotation by angles θ and φ, and (f_x, f_y, f_z) denotes the frequency component in the spatial-spectral dimension [22]. The three-dimensional Gabor filter spatial model is shown in Fig 2.

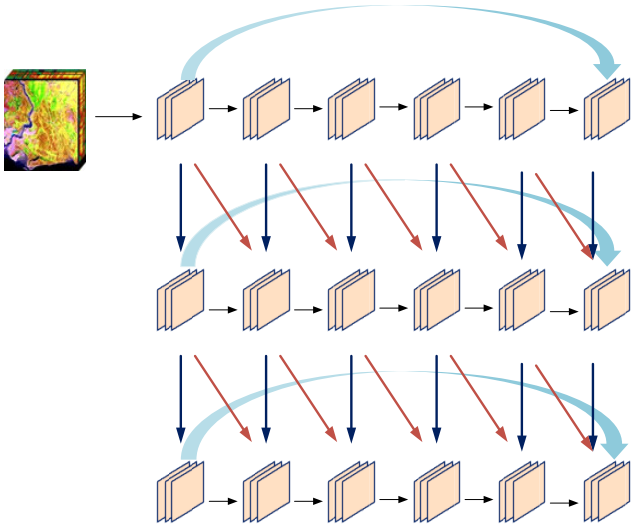

FIGURE 1. Multi-scale dense network (MSDN) architecture.

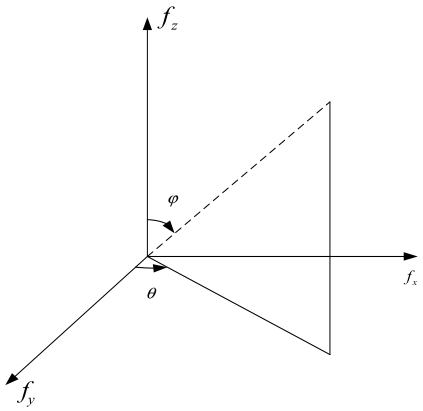

FIGURE 2. Spatial model of three-dimensional Gabor filte.

FIGURE 3. 3D Gabor filter pre-processing flow chart.

The hyperspectral raw image data is fed into a 3D Gabor filter, and a new 3D cube data is obtained after convolution to take the real part. The equation is

$$\mathrm{HSI}_{texture} = \mathrm{HSI}\,(x, y, z) \otimes G\,(x, y, z) \tag{2}$$

where $\mathrm{HSI}\,(x, y, z)$ denotes the original hyperspectral data set, and $G\,(x, y, z)$ denotes the 3D Gabor filter in a certain direction. By adjusting the values of θ and φ of the filters, a three-dimensional Gabor filter with different orientations can be obtained, and the filters with different orientations are combined to form a filter bank. The flowchart of 3D Gabor filter for extracting hyperspectral remote sensing image features is shown in Fig 3.

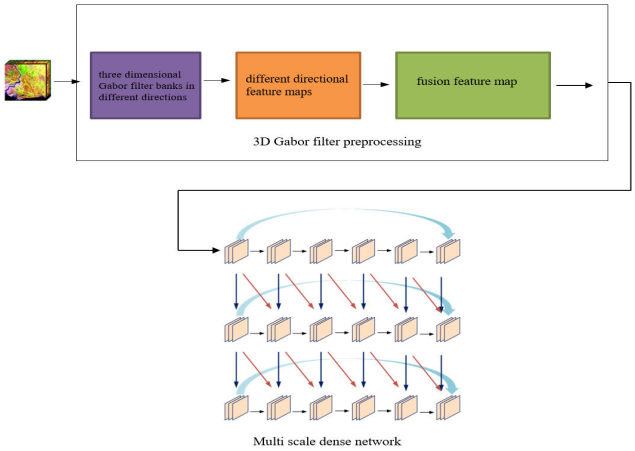

FIGURE 4. Network structure of MSDN hyperspectral remote sensing image classifier based on 3D Gabor filter.

By preprocessing the original hyperspectral images with filters of different orientations, feature information of different scales and orientations can be obtained, and finally these features are fused using linear superposition, and the fused feature information is used in the multi-scale dense network, thus avoiding deepening of the deep learning network and realizing the optimization of the multi-scale dense network. The multi-scale dense network classification method based on Gabor filter can effectively improve the accuracy of classification, especially in processing hyperspectral images with complex textures.

C. THREE-DIMENSIONAL GABOR FILTER AND MULTI-SCALE DENSE NETWORK

The Gabor filter-based MSDN hyperspectral remote sensing image classification method is shown in Fig 4. First, according to the three-dimensional Gabor filter definition equation (3).

$$\begin{aligned} G(x, y, z) = & \frac{1}{(2\pi)^{3/2}\sigma_x\sigma_y\sigma_z} \\ & \times \exp\left(-\frac{1}{2}\left(\left(\frac{x'}{\sigma_x}\right)^2 + \left(\frac{y'}{\sigma_y}\right)^2 + \left(\frac{z'}{\sigma_z}\right)^2\right)\right) \\ & \times \exp\left(2i\pi\left(xf_x + yf_y + zf_z\right) + \varphi\right) \end{aligned} \tag{3}$$

where $x' = x\cos\theta + y\sin\theta$, $y' = -x\cos\theta + y\sin\theta$, $z' = z$ can be seen by varying the 3-D Gabor filters θ and φ, which can be obtained in different directions. In order to fully extract the texture features in each direction in the hyperspectral raw image and to take into account the reduction of the computational effort of the 3D Gabor filter, the paper is adjusted in steps of $\frac{\pi}{4}$ within $(0, \pi)$ for θ and φ. Since the frequency component does not change with θ when φ is 0, it is sufficient to take a direction at this point.

The paper uses 13 directions of Gabor filters, of which θ and φ are respectively$(\theta = 0, \varphi = 0)$, $(\theta = 0, \varphi = \frac{\pi}{4})$, $(\theta = \frac{\pi}{4}, \varphi = \frac{\pi}{4})$, $(\theta = \frac{\pi}{2}, \varphi = \frac{\pi}{4})$, $(\theta = \frac{3\pi}{4}, \varphi = \frac{\pi}{4})$, $(\theta =$

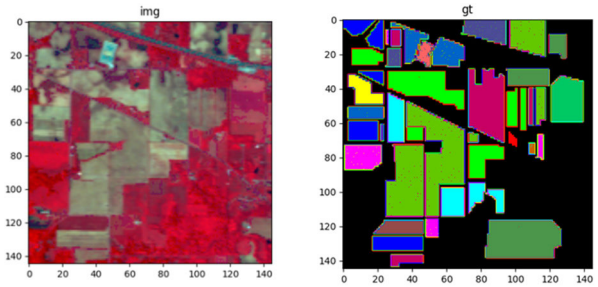

FIGURE 5. (a) Pseudo-color plot of the Indian Pines dataset, (b) Calibration plot of the Indian Pines dataset.

$0, \varphi = \frac{\pi}{2}), (\theta = \frac{\pi}{4}, \varphi = \frac{\pi}{2}), (\theta = \frac{\pi}{2}, \varphi = \frac{\pi}{2}), (\theta = \frac{3\pi}{4}, \varphi = \frac{\pi}{2}), (\theta = 0, \varphi = \frac{3\pi}{4}), (\theta = \frac{\pi}{4}, \varphi = \frac{3\pi}{4}), (\theta = \frac{\pi}{2}, \varphi = \frac{3\pi}{4}), (\theta = \frac{3\pi}{4}, \varphi = \frac{3\pi}{4})$.

Then, the extracted features in 13 directions are fused using linear superposition so that a new 3D feature data containing all feature information is generated. The new 3D feature information data is then fed into the multi-scale dense network model for deep feature extraction. The multi-scale dense network uses two convolutional kernels, and the learning rate is set to 0.001. The network has three scales with 6, 12, and 6 layers of convolution on each of the three scales. Finally, a Softmax classifier is used to classify and obtain the classification results.

D. EVALUATION INDICATORS

The three evaluation metrics used in the paper are Overall Accuracy (OA), Average Accuracy (AA), and Kappa coefficient.

The OA calculation formula is

$$\mathrm{OA} = \frac{\sum_{i=1}^{k} P(i,i)}{N} \tag{4}$$

where k denotes the number of categories; N denotes the total number of test samples; $P(i,i)$ denotes the number of the ith category correctly classified.

The AA calculation formula is

$$\mathrm{AA} = \frac{\sum_{i=1}^{k} \mathrm{OA}_i}{k} \tag{5}$$

where OA_i denotes the total classification accuracy of class i.

The Kappa calculation formula is

$$\mathrm{Kappa} = \frac{N \sum_{i=1}^{k} P(i,i) - \sum_{i=1}^{k} P(i,) P(,i)}{N^2 - \sum_{i=1}^{k} P(i,) P(,i)} \tag{6}$$

where $P(i,), P(,i)$ denote the total number of test samples in row i and column i, respectively.

III. EXPERIMENTS AND RESULTS

A. EXPERIMENTAL DATA SET

The Indian Pines dataset (abbreviation: IP) was imaged by the Visual Infrared Imager (AVIRIS) in 1992 on a piece of Indian pine in Indiana, USA, and then intercepted at a size of 145 × 145 for labeling as a hyperspectral image classification test purpose [18]. Imaging wavelength range 0.4-2.5μm, spectral resolution of 10μm, spatial resolution of 20m, is in the continuous 220 band continuous imaging of the ground, but the use of 20 cannot be water reflection of the band, leaving 200 bands as the object of study. There are 16 types of features in the dataset, and the samples are unevenly distributed, and the sample distribution is shown by Table 2. The pseudo color images and calibration maps of the dataset are shown by Fig 5(a) and (b).

TABLE 2. Sample size of Indian Pines dataset.

No.	Name	Number
1	Alfalfa	46
2	Corn-notill	1428
3	Corn-mintill	830
4	Corn	237
5	Grass-pasture	483
6	Grass-trees	730
7	Grass-pasture-mowed	28
8	Hay-windrowed	478
9	Oats	20
10	Soybean-notill	972
11	Soybean-mintill	2455
12	Soybean-clean	593
13	Wheat	205
14	Woods	1265
15	Buildings-Grass-Trees-Drives	386
16	Stone-Steel-Towers	93

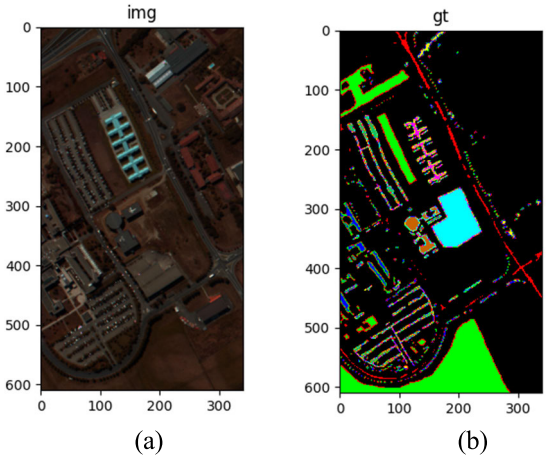

FIGURE 6. (a) Pseudo-color plot of the Pavia University dataset, (b) Calibration plot of the Pavia University dataset.

The Pavia University dataset (abbreviation: PU) was acquired by the Airborne Optical Spectral Imager (ROSIS) in 2003 at the University of Pavel, Italy, in the wavelength range 0.43-0.86 μm [19]. was used for hyperspectral image classification. The sensor has a total of 115 bands, and after processing the data retains 103 bands, the data and size is

TABLE 3. Sample size of Pavia University dataset.

No.	Name	Number
1	Alfalfa	46
2	Corn-notill	1428
3	Corn-mintill	830
4	Corn	237
5	Grass-pasture	483
6	Grass-trees	730
7	Grass-pasture-mowed	28
8	Hay-windrowed	478
9	Oats	20
10	Soybean-notill	972
11	Soybean-mintill	2455
12	Soybean-clean	593
13	Wheat	205
14	Woods	1265
15	Buildings-Grass-Trees-Drives	386
16	Stone-Steel-Towers	93

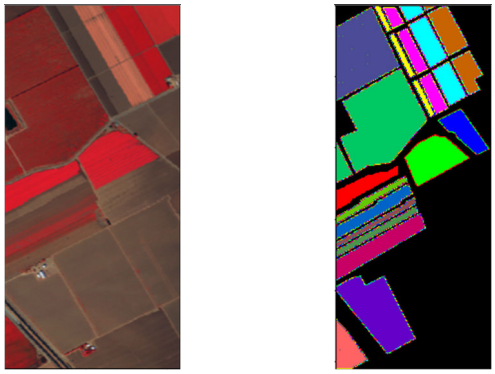

(a) (b)

FIGURE 7. (a) Pseudo-color plot of the Salinas dataset, (b) Calibration plot of the Salinas dataset.

610 × 340 including 9 classes of features, and the sample distribution is shown by Table 3. The pseudo-color images and calibration maps of the dataset are shown by Fig 6 (a) and (b).

The Salinas dataset was taken by the AVIRIS sensor in Salinas Valley, California, with a dataset size of 512 × 217 and a spatial resolution of 3.7 m [20]. It contains 224 continuous bands, and the actual bands used for training are 204 by removing 20 absorption bands. There are 16 feature types in the study area, and the sample distribution is shown by Table 4. The pseudo-color images and calibration maps of the dataset are shown by Fig 7(a) and (b).

B. EXPERIMENTAL CONFIGURATION AND ANALYSIS OF EXPERIMENTAL RESULTS

The experiments were conducted using the same hardware platform, with Linux Ubuntu 18.04.5 LTS system as the operating platform and two Intel® Xeon® processor E5-2698v 42.2GHz, 50M cache, 9.60GT/s QPI,Tuibo,HT,20C/40T (135W), 256GB memory capacity. NVIDIA A100 Tensor Core GPU with up to 320GB of total GPU memory. The PYTORCH framework was used for deep learning. 10% and 90% of the experimental data were randomly divided into training and test groups, respectively, with epoch=200 and learning rate lr=0.001 for the experiments.

The feature information extracted from the 3D Gabor filter with 13 different directions is linearly superimposed, and the new feature information after fusion is input into the multi-scale dense network to obtain the classification results. The classification results are also compared with SVM, 3D-CNN [21], HybirdSN [22] and MSDN, as shown in Table 5 and Fig 8.

TABLE 4. Sample size of Salinas dataset.

No.	Name	Number
1	Brocoli_green_weeds_1	2009
2	Brocoli_green_weeds_2	3726
3	Fallow	1976
4	Fallow_rough_plow	1394
5	Fallow_smooth	2678
6	stubble	3959
7	Celery	3579
8	Grapes_untrained	11271
9	Soil_vineyard_develop	6203
10	Corn _senesced _green _weeds	3278
11	Lettuce_romaine_4wk	1068
12	Lettuce_romaine_5wk	1927
13	Lettuce_romaine_6wk	916
14	Lettuce_romaine_7wk	1070
15	Vinyard_untrained	7268
16	Vinyard_vertical_trellis	1807

TABLE 5. Classification accuracy of different methods for IP dataset (%).

No.	Method				
	SVM	3D-CNN	HybirdSN	MSDN	Gabor-MSDN
1	100	97	100	95	100
2	90	98	96	100	100
3	72	98	98	98	100
4	92	97	98	100	99
5	98	99	99	99	100
6	95	99	98	100	100
7	67	89	100	100	100
8	100	100	99	100	100
9	50	100	76	94	96
10	72	100	99	100	100
11	86	99	96	98	100
12	80	98	98	99	100
13	100	100	98	99	100
14	98	100	99	100	100
15	59	96	99	100	100
16	90	98	93	91	100
OA	86.52	98.23	97.47	99.10	99.91
AA	84.28	98.80	96.05	97.96	99.88
Kappa	84.59	97.31	97.12	98.97	99.90

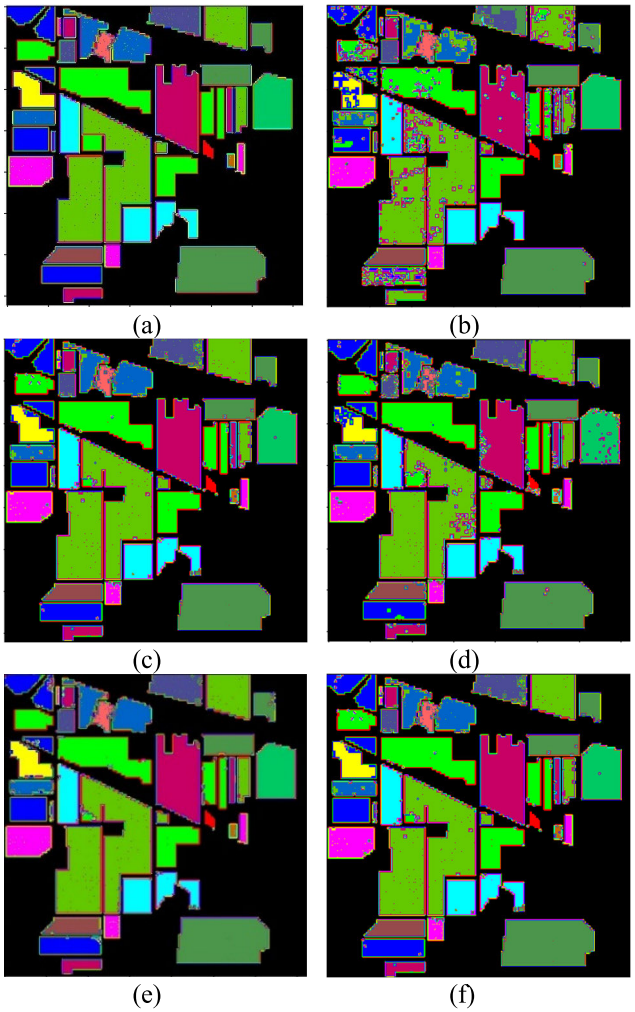

FIGURE 8. Classification results of IP dataset (a) labeled images, (b) SVM, (c) 3D-CNN, (d) HybirdSN. (e)MSDN, (f)Gabor-MSDN.

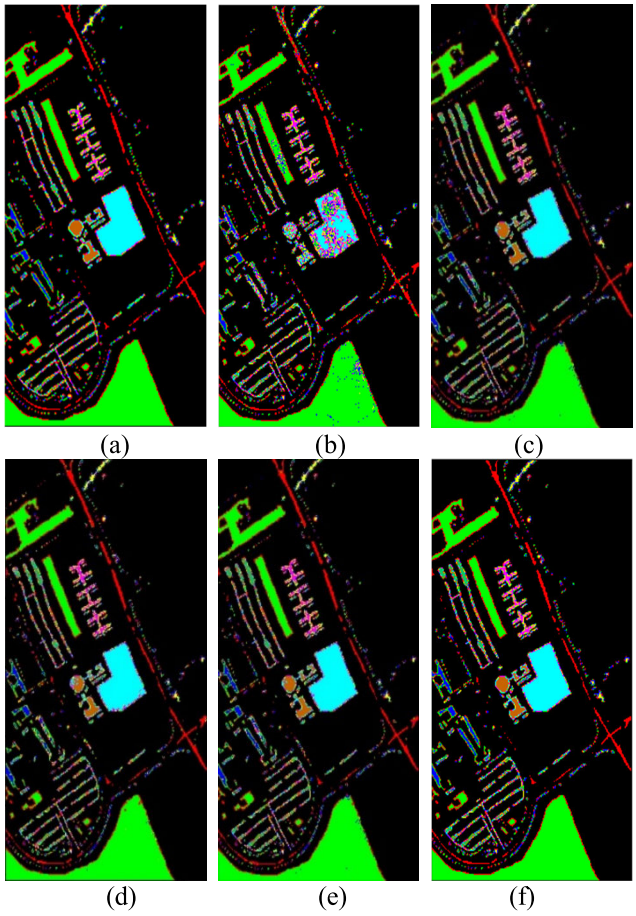

FIGURE 9. Classification results of PU dataset (a) labeled images, (b) SVM, (c) 3D-CNN, (d) HybirdSN. (e)MSDN, (f)Gabor-MSDN.

TABLE 6. Classification accuracy of different methods for PU dataset (%).

No.	Method				
	SVM	3D-CNN	HybirdSN	MSDN	Gabor-MSDN
1	96	99	99	100	100
2	98	100	100	100	100
3	80	99	99	99	100
4	88	100	99	93	100
5	100	100	100	100	99
6	81	100	100	99	100
7	64	99	99	100	98
8	90	98	98	99	99
9	100	99	99	93	96
OA	92.55	98.47	99.57	98.95	99.54
AA	88.74	99.28	98.90	98.24	98.94
Kappa	90.01	98.97	99.43	98.62	99.39

As can be seen from Table 5, the method proposed in this paper outperforms the comparison method in the IP database. Compared with the SVM, 3D-CNN, HybirdSN and MSDN methods, this method achieves an OA value of 99.91% with gains of 13.39%, 1.68%, 2.44% and 0.81%, respectively. In addition, it is worth noting that for the classes with only a small number of training samples (Class 7 and Class 9), other methods suffer from more serious classification errors when faced with only a small number of training samples in the IP. Instead, the method showed better performance on both samples, suggesting that Gabor-MSDN was able to extract the features of both samples more adequately.

(2) Experimental results of Pavia University dataset

The feature information extracted from the 3D Gabor filter with 13 different directions is linearly superimposed, and the new feature information after fusion is input into the multi-scale dense network to obtain the classification results. The classification results are also compared with SVM, 3D-CNN [21], HybirdSN [22] and MSDN, as shown in Table 6 and Fig 9.

The feature information extracted from the 3D Gabor filter in 13 different directions is linearly superimposed, and the new feature information after fusion is input into the multi-scale dense network to obtain the classification results. The classification results are also compared with SVM, 3D-CNN, HybirdSN and MSDN, as shown in Table 7 and Fig 10.

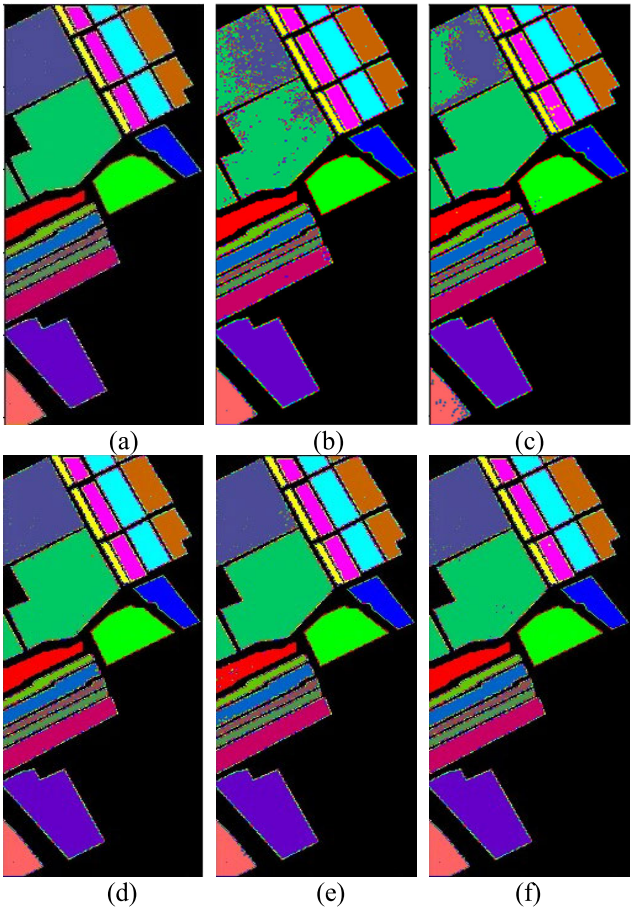

FIGURE 10. Classification results of Salinas dataset (a) labeled images, (b) SVM, (c) 3D-CNN, (d) HybirdSN. (e)MSDN, (f)Gabor-MSDN.

TABLE 7. Classification accuracy of different methods for Salinas dataset (%).

	Method				
No.	SVM	3D-CNN	HybirdSN	MSDN	Gabor-MSDN
1	100	100	100	100	100
2	100	100	100	100	100
3	99	100	100	100	100
4	99	99	100	99	100
5	100	100	100	100	100
6	100	100	100	100	100
7	100	100	100	100	100
8	91	100	100	100	100
9	100	100	100	100	100
10	97	100	100	100	100
11	99	99	100	100	100
12	100	100	100	100	100
13	100	99	100	100	100
14	97	100	100	100	100
15	64	100	100	100	100
16	98	100	100	100	100
OA	92.73	99.85	99.94	99.91	99.96
AA	96.41	99.79	99.90	99.92	99.93
Kappa	91.88	99.84	99.93	99.90	99.95

The results on the Salinas dataset similarly show that the classification accuracy of the Gabor-MSDN method proposed in this paper lies in the first place compared to other methods. Compared with the SVM, 3D-CNN, HybirdSN and MSDN methods, the method achieves an OA value of 99.96% with gains of 7.23%, 0.11%, 0.02% and 0.08%, respectively. Therefore, the proposed method in this paper also achieves good classification performance on the Salinas dataset.

TABLE 8. Classification results of different models combined with Gabor filters (%).

	Method					
	Gabor-3D-CNN			Gabor-HybirdSN		
No.	IP	PU	SA	IP	PU	SA
1	100	100	100	100	100	100
2	100	100	100	99	100	100
3	99	100	100	98	100	100
4	99	98	99	98	99	100
5	99	100	100	96	100	100
6	99	100	100	96	100	100
7	96	98	100	99	99	100
8	100	99	100	100	99	100
9	100	99	100	99	99	100
10	99		100	100		100
11	97		100	99		100
12	98		100	98		100
13	100		100	97		100
14	100		100	100		100
15	100		100	99		100
16	90		100	92		100
OA	98.72	99.56	99.88	98.27	99.75	99.94
AA	95.57	98.92	99.80	96.61	99.27	99.90
Kappa	97.82	99.41	99.87	98.02	99.67	99.93

In order to further prove that 3D Gabor can further extract the features of hyperspectral remote sensing images, the proposed 3D Gabor filter bank is fused with common hyperspectral classification models for the experiment, and the classification results are shown in Table 8. As can be seen from Table 8, the classification results of IP, PU and SA datasets after 3D Gabor filter feature extraction followed by 3D-CNN, HybirdSN network model are improved in OA, AA and Kappa coefficients.

IV. CONCLUSION

The MSDN hyperspectral remote sensing image classification method based on 3D Gabor filters proposed in this paper firstly preprocesses the hyperspectral remote sensing images by using thirteen 3D Gabor filter sets with different directions and scales, and then inputs the preprocessed data into a multi-scale dense network with better feature extraction and feature fusion capabilities for feature extraction. Through the simulation results of classification of three publicly available hyperspectral remote sensing datasets, it can be seen that the method in this paper solves the problems of multi-scale dense network with complex network structure and more network parameters leading to the degradation of classification efficiency, and with the deepening and widening of the

network there will be gradient explosion and low classification accuracy of small samples. Moreover, by comparing with SVM, 3D-CNN, HybirdSN and MSDN classification methods, it can be seen that the multi-scale dense network with the introduction of 3D Gabor filter has higher classification accuracy, which proves the effectiveness of the proposed method.

REFERENCES

[1] C.-I. Chang, X.-L. Zhao, M. L. G. Althouse, and J. Jong Pan, "Least squares subspace projection approach to mixed pixel classification for hyperspectral images," *IEEE Trans. Geosci. Remote Sens.*, vol. 36, no. 3, pp. 898–912, May 1998, doi: 10.1109/36.673681.

[2] F. Melgani and L. Bruzzone, "Classification of hyperspectral remote sensing images with support vector machines," *IEEE Trans. Geosci. Remote Sens.*, vol. 42, no. 8, pp. 1778–1790, Aug. 2004, doi: 10.1109/TGRS.2004.831865.

[3] Y. Chen, Z. Lin, X. Zhao, G. Wang, and Y. Gu, "Deep learning-based classification of hyperspectral data," *IEEE J. Sel. Topics Appl. Earth Observ. Remote Sens.*, vol. 7, no. 6, pp. 2094–2107, Jun. 2014, doi: 10.1109/JSTARS.2014.2329330.

[4] J. Yue, W. Zhao, S. Mao, and H. Liu, "Spectral–spatial classification of hyperspectral images using deep convolutional neural networks," *Remote Sens. Lett.*, vol. 6, no. 6, pp. 468–477, Jun. 2015, doi: 10.1080/2150704X.2015.1047045.

[5] X. Xu, W. Li, Q. Ran, Q. Du, L. Gao, and B. Zhang, "Multisource remote sensing data classification based on convolutional neural network," *IEEE Trans. Geosci. Remote Sens.*, vol. 56, no. 2, pp. 937–949, Feb. 2018, doi: 10.1109/TGRS.2017.2756851.

[6] S. Bera, V. K. Shrivastava, and S. C. Satapathy, "Advances in hyperspectral image classification based on convolutional neural networks: A review," *Comput. Model. Eng. Sci.*, vol. 133, no. 2, pp. 219–250, 2022.

[7] A. Krizhevsky, I. Sutskever, and G. E. Hinton, "ImageNet classification with deep convolutional neural networks," in *Proc. Adv. Neural Inf. Process. Syst.*, vol. 25. Lake Tahoe, NV, USA: Harrahs and Harveys, 2012.

[8] L. Jiao, M. Liang, H. Chen, S. Yang, H. Liu, and X. Cao, "Deep fully convolutional network-based spatial distribution prediction for hyperspectral image classification," *IEEE Trans. Geosci. Remote Sens.*, vol. 55, no. 10, pp. 5585–5599, Oct. 2017, doi: 10.1109/TGRS.2017.2710079.

[9] C. Szegedy, W. Liu, Y. Jia, P. Sermanet, S. Reed, D. Anguelov, D. Erhan, V. Vanhoucke, and A. Rabinovich, "Going deeper with convolutions," in *Proc. IEEE Conf. Comput. Vis. Pattern Recognit. (CVPR)*, Boston, MA, USA, Jun. 2015, pp. 1–9.

[10] K. He, X. Zhang, S. Ren, and J. Sun, "Deep residual learning for image recognition," in *Proc. IEEE Conf. Comput. Vis. Pattern Recognit. (CVPR)*, Las Vegas, NV, USA, Jun. 2016, pp. 770–778.

[11] J. Shen, Z. Zheng, Y. Sun, M. Zhao, Y. Chang, Y. Shao, and Y. Zhang, "HAMNet: Hyperspectral image classification based on hybrid neural network with attention mechanism and multi-scale feature fusion," *Int. J. Remote Sens.*, vol. 43, no. 11, pp. 4233–4258, Jun. 2022.

[12] Z. Li, T. Wang, W. Li, Q. Du, C. Wang, C. Liu, and X. Shi, "Deep multilayer fusion dense network for hyperspectral image classification," *IEEE J. Sel. Topics Appl. Earth Observ. Remote Sens.*, vol. 13, pp. 1258–1270, 2020, doi: 10.1109/JSTARS.2020.2982614.

[13] C. Zhang, G. Li, and S. Du, "Multi-scale dense networks for hyperspectral remote sensing image classification," *IEEE Trans. Geosci. Remote Sens.*, vol. 57, no. 11, pp. 9201–9222, Nov. 2019, doi: 10.1109/TGRS.2019.2925615.

[14] Z. Xu, H. Yu, K. Zheng, L. Gao, and M. Song, "A novel classification framework for hyperspectral image classification based on multiscale spectral–spatial convolutional network," in *Proc. 11th Workshop Hyperspectral Imag. Signal Process., Evol. Remote Sens. (WHISPERS)*, Amsterdam, The Netherlands, 2021, pp. 1–5, doi: 10.1109/WHISPERS52202.2021.9483998.

[15] H. Fırat, M. E. Asker, M. İ. Bayındır, and D. Hanbay, "Hybrid 3D/2D complete inception module and convolutional neural network for hyperspectral remote sensing image classification," *Neural Process. Lett.*, vol. 55, no. 2, pp. 1087–1130, Apr. 2023, doi: 10.1007/s11063-022-10929-z.

[16] A. Ari, "Multipath feature fusion for hyperspectral image classification based on hybrid 3D/2D CNN and squeeze-excitation network," *Earth Sci. Informat.*, vol. 16, no. 1, pp. 175–191, Mar. 2023, doi: 10.1007/s12145-022-00929-x.

[17] L. He, C. Liu, J. Li, Y. Li, S. Li, and Z. Yu, "Hyperspectral image spectral–spatial-range Gabor filtering," *IEEE Trans. Geosci. Remote Sens.*, vol. 58, no. 7, pp. 4818–4836, Jul. 2020, doi: 10.1109/TGRS.2020.2967778.

[18] J. Wang, "A novel collaborative representation algorithm for spectral unmixing of hyperspectral remotely sensed imagery," *IEEE Access*, vol. 9, pp. 89243–89248, 2021, doi: 10.1109/ACCESS.2021.3085398.

[19] Q. Li, B. Zheng, and Y. Yang, "Spectral–spatial active learning with structure density for hyperspectral classification," *IEEE Access*, vol. 9, pp. 61793–61806, 2021, doi: 10.1109/ACCESS.2021.3074405.

[20] X. Hu, Y. Zhong, X. Wang, C. Luo, J. Zhao, L. Lei, and L. Zhang, "SPNet: Spectral patching end-to-end classification network for UAV-borne hyperspectral imagery with high spatial and spectral resolutions," *IEEE Trans. Geosci. Remote Sens.*, vol. 60, 2022, Art. no. 5503417, doi: 10.1109/TGRS.2021.3049292.

[21] Y. Li, H. Zhang, and Q. Shen, "Spectral–spatial classification of hyperspectral imagery with 3D convolutional neural network," *Remote Sens.*, vol. 9, no. 1, p. 67, Jan. 2017.

[22] S. K. Roy, G. Krishna, S. R. Dubey, and B. B. Chaudhuri, "HybridSN: Exploring 3-D–2-D CNN feature hierarchy for hyperspectral image classification," *IEEE Geosci. Remote Sens. Lett.*, vol. 17, no. 2, pp. 277–281, Feb. 2020.

CHAOZHU ZHANG received the B.S. degree in electronic engineering from the Harbin Institute of Technology, Harbin, China, in 1993, and the M.S. and Ph.D. degrees in communication and information systems from Harbin Engineering University, Harbin, in 2002 and 2006, respectively.

His research interests include the research of signal processing applications in radar and communication, machine learning, and edge computing.

SHENGRONG ZHU received the bachelor's degree in electronic information from the Qilu University of Technology (Shandong Academy of Sciences), Jinan, China, in 2023.

DAN XUE received the B.S. degree in communication engineering from the Qilu University of Technology (Shandong Academy of Sciences), Jinan, China, in 2021, where she is currently pursuing the master's degree in new generation of electronic information technology with the Department of Electrical, Electronics and Control.

Her research interests include deep learning and hyperspectral image classification.

SONG SUN received the B.S. degree in communication engineering from the Qilu University of Technology (Shandong Academy of Sciences), Jinan, China, in 2021, where he is currently pursuing the master's degree in new generation of electronic information technology with the Department of Electrical Electronics and Control.

His research interest includes microcontrollers.